JOURNAL OF SPACECRAFT AND ROCKETS
Vol. 56, No. 5, September–October 2019

Novel Approach for Mars Entry Blackout Elimination Based on X-Ray Communication

Shuang Hang,* Xiaobin Tang,† Huan Li,* Yunpeng Liu,‡ Junxu Mu,* and Wei Zhou*
Nanjing University of Aeronautics and Astronautics, 210016 Nanjing, People's Republic of China

DOI: 10.2514/1.A34421

An approach is presented for eliminating communication blackout caused by the plasma sheath encountered during the Mars atmospheric entry phase. On the basis of the high penetration of X-ray beams, the expectation was to avoid communication interruptions by establishing an X-ray communication link between the Mars orbiter and the entry vehicle. In this study, the plasma penetration performance of X-rays is evaluated based on the numerical method. The transmission properties of an X-ray beam in the Martian atmosphere were assessed based on the Monte Carlo simulation. The performance of X-ray communication links in the blackout region is evaluated, and the minimum transmitting power required for low bit-error-rate communication is obtained. The results show that an X-ray beam can not only pass through the plasma sheath generated during the atmospheric entry phase without attenuation but also penetrate the atmosphere and establish a stable communication link between a Mars orbiter and the entry vehicle.

Nomenclature

A_R = area of the receiving antenna, m^{-2}
Att = attenuation coefficient
B = communication bandwidth, Hz
C_t = transmission coefficient of atmospheric and plasma environment
c = velocity of light, m/s
D_x = component of electric displacement density in the x direction
E_x = electric component in the x direction
e = electron charge, C
F_B = background X-ray flux, $m^{-2} \cdot s^{-1}$
f_c = frequency of the electromagnetic wave, GHz
H_y = magnetic component in the y direction
h = Planck constant
i_d = dark current of the X-ray detector, A
k = propagation vector
L = communication distance, m
M = modulation level of pulse position modulation method
m = number of steps in space
m_e = mass of the electron, kg
N_c = critical electron density, m^{-3}
N_e = electron density, m^{-3}
$N_{e,1}$ = critical plasma density of the ultrahigh frequency, m^{-3}
$N_{e,2}$ = critical plasma density of the S band, m^{-3}
$N_{e,3}$ = critical plasma density of the X band, m^{-3}
$N_{e,4}$ = critical plasma density of the Ka band, m^{-3}
$N_{e,5}$ = peak value of electron density during the Mars atmospheric entry phase, m^{-3}
$N_{\max}$ = peak value of the plasma electron density, m^{-3}
n = number of steps in time
P_R = receiving power of the X-ray communication receiver, W
P_T = transmitting power of the X-ray communication transmitter, W
T = transmission coefficient
v = frequency of an X-ray, Hz
v_c = electron collision frequency, GHz
w_p = plasma frequency, rad/s
z_0 = location of the boundary layer, m
z_1 = thickness of the plasma sheath, m
Δt = temporal step size, s
Δz = spatial step size, m
ε = effective dielectric coefficient of the plasma sheath, F/m
ε_0 = permittivity of free space, F/m
η = efficiency of an X-ray detector
η_c = efficiency of X-ray-focusing optics
θ = angle between the X-ray communication link and the vertical line, deg
θ_d = beam angle of the transmitting antenna, rad
λ = wavelength of the carrier, m
ω = angular frequency of the incident X-ray, rad/s

I. Introduction

THE Mars landing mission is one of the hotspots in future deep space exploration [1,2]. During the Mars landing, the atmospheric entry phase is highly unpredictable and dangerous, causing entry vehicles to undergo peak heating and peak dynamic pressure [3,4]. The most critical thing is that the lander will encounter tens of seconds of communication disruption in this phase, which is called communication blackout.

During the Mars atmospheric entry phase, especially at hypersonic conditions, shock waves form in front of the vehicle and heat the atmospheric gas. As a result, carbon dioxide and nitrogen gas molecules become dissociated and ionized. Plasma is generated by the ionization of atmospheric gases and ablation of the heat shield. The electron number density of the generated plasma layer could reach up to 10^{19} m^{-3} [5]. The plasma surrounding the spacecraft attenuates the communication signals due to the weak penetration of electromagnetic (EM) waves in the RF frequency [6–8]. Tens of seconds of the communication blackout in the Mars atmospheric entry phase caused by the plasma sheath have been observed in previous Mars landing missions. Therefore, a communication method that cannot be hindered by the plasma sheath is highly necessary [9].

In this study, a scheme that maintains continuous data transmission between lander and orbiter by X-ray communication (XCOM) links

Received 23 October 2018; revision received 12 March 2019; accepted for publication 17 April 2019; published online 28 June 2019.

*Graduate Student, Department of Nuclear Scienceand Engineering, 29 Yudao Street, Jiangsu; also MIIT Key Laboratory of Material Preparation and Protection Technology for Harsh Environment, 211106 Nanjing, People's Republic of China.

†Professor, Department of Nuclear Scienceand Engineering, 29 Yudao Street, Jiangsu; also MIIT Key Laboratory of Material Preparation and Protection Technology for Harsh Environment, 211106 Nanjing, People's Republic of China.

‡Assistant Professor, Department of Nuclear Science and Engineering, 29 Yudao Street, Jiangsu; also MIIT Key Laboratory of Material Preparation and Protection Technology for Harsh Environment, 211106 Nanjing, People's Republic of China.

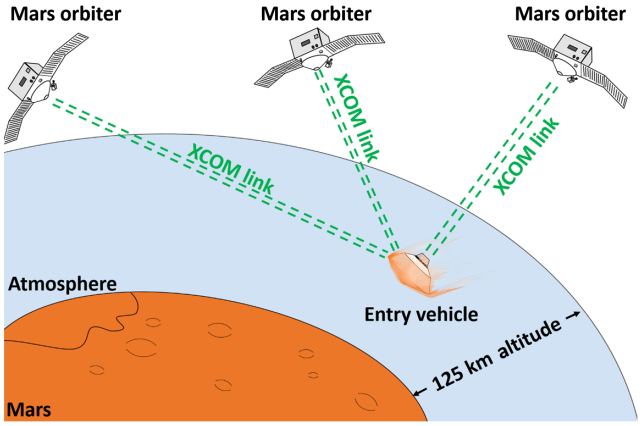

Fig. 1 Schematic of XCOM in Mars atmospheric entry phase.

during the Mars atmospheric entry phase is proposed. XCOM is a new mode of communication that uses the X-ray as a carrier and is expected to eliminate the communication blackout due to its high penetrability [10]. Figure 1 presents a schematic of XCOM during the Mars atmospheric entry phase. Both the Mars orbiter and the entry vehicle carry the XCOM system consisting of a transmitter and a receiver. The entry vehicle flies through the atmosphere and is surrounded by the plasma sheath that blocks RF signals. With the high penetration of X-ray beams, a stable XCOM link between the entry vehicle and the orbiter can be established. The XCOM link can be used to transmit the entry vehicle's status information, and more importantly, it is expected to be used for providing navigation for landers during Mars entry. Researchers have proposed a precise navigation system based on the radio communication link between the lander and the orbiter, which is expected to give the lander the capability of pinpoint landing [3,11–13]. XCOM links can also be employed to achieve the same goal. During the Mars atmospheric entry, the Mars orbiter sends its position coordinates and ranging codes to the entry vehicle in real time. On the basis of pseudorange measurement, the distance between the Mars orbiter and the entry vehicle can be obtained. If the X-ray signals from three orbiters can be received simultaneously, the entry vehicle can determine its position by processing the position coordinates and pseudodistance information of the three orbiters. The entry vehicle's velocity and trajectory can then be determined by continuous position measurement. Furthermore, by modifying the trajectory of the entry vehicle, the landing error can be reduced. If the XCOM system works independently and the entry vehicle carries a precise atomic clock, then three orbiters are needed to realize Mars entry navigation. However, integrating the XCOM-based navigation system with an inertial navigation system can reduce the number of orbiters required for positioning. In this XCOM-based positioning scheme, the system consists of a modulated X-ray source, a high-time-resolution X-ray detector, and X-ray-focusing optics [10]. The modulated X-ray source in the transmitter is used to generate the pulsed X-ray beam carrying information and ranging codes. The X-ray detector in the receiver is used to detect the X-ray signal from the transmitter [14]. The nested X-ray-focusing optics are used as the transmitting and receiving antennas. In addition, the acquisition pointing and tracking system is required to keep both ends of XCOM aligned.

In previous studies, the applicability of XCOMs in the Earth's upper atmosphere has been simply analyzed. However, due to different atmospheric and plasma parameters, the applicability of XCOM in the Mars atmospheric entry phase needs to be verified. As shown in Fig. 1, the modulated X-ray beam emitted from the entry vehicle first passes through the plasma sheath. The X-ray beam then propagates through the Martian upper atmosphere and is eventually received by the orbiter. Therefore, we evaluate the transmission property of X-ray beams in the plasma and atmosphere and assess communication performance.

II. Interaction Between Electromagnetic Waves and the Plasma Sheath

When EM waves propagate through the plasma sheath surrounding the entry vehicle, they are reflected and absorbed by the ions and electrons in the plasma if the plasma is sufficiently dense. During this process, the free electrons in the plasma play a major role in reflecting and absorbing the EM waves. The transmission performance of the EM waves depends on frequency f_c and plasma frequency w_p. Plasma frequency w_p and critical electron density N_c can be determined by the following equations:

$$w_p = \sqrt{e^2 N_e/\varepsilon_0 m_e} \tag{1}$$

$$N_c = f_c^2 \varepsilon_0 m_e / e^2 \tag{2}$$

Theoretically, the carrier can penetrate the plasma sheath when its frequency is higher than the plasma frequency or when the electron density of the plasma is lower than the critical electron density. N_e depends on the entry vehicle's shape, velocity, trajectory, altitude, and attack angle; and it is nonuniformly distributed. Considering the plasma sheath as an anisotropic nonmagnetized cold plasma with collision, it can be described by N_e and v_c [15,16]. $N_e(z)$ distributed outward from the spacecraft surface satisfies the following double Gaussian function:

$$N_e(z) = \begin{cases} N_{\max} \exp(-c_1(z-z_0)^2) & (0 \le z \le z_0) \\ N_{\max} \exp(-c_2(z-z_0)^2) & (z_0 \le z \le z_1) \end{cases} \tag{3}$$

Coefficients c_1 and c_2 determine the shape of the distribution. Parameters $c_1 = 1$, $c_2 = 0.5$, $z_0 = 5$ cm, and $z_1 = 15$ cm were set in our study [5,17,18]. In addition, we employed $N_{\max}$ in the range of 1.99×10^{15}–1.27×10^{19} m^{-3} and v_c in the range of 0.01–10 GHz [19,20].

A. Simulation Method

The finite difference time domain (FDTD) [21,22] and Wentzel–Kramer–Brillouin (WKB) [23] methods have been widely used to simulate the EM wave propagation process in plasma media. The transmission performances of different carriers, including the RF band and X-ray, were evaluated to verify the high penetration of X-ray under the plasma condition during the Mars atmospheric entry.

In this study, a one-dimensional shift operator FDTD (SO-FDTD) was employed to simulate the plane wave that normally impinges on a double Gaussian distributed and nonmagnetized collision plasma slab [21,24]. For the simulation based on the one-dimensional FDTD method, the EM wave traveling in the z direction could be represented by the electric or magnetic component in the x or y direction. The discrete recursive relationships among a magnetic component in the y direction H_y, a component of electric displacement density in the x direction D_x, and an electric component in the x direction E_x, respectively, satisfy the following equations (Ref. [21]):

$$H_y^{n+(1/2)}\left(m+\frac{1}{2}\right) = H_y^{n-(1/2)}\left(m+\frac{1}{2}\right) - \frac{\Delta t}{\mu_0 \Delta z} \cdot [E_x^n(m+1) - E_x^n(m)] \tag{4}$$

$$D_x^{n+1}(m) = D_x^n(m) - \frac{\Delta t}{\varepsilon_0 \Delta z}\left(H_y^{n+(1/2)}\left(m+\frac{1}{2}\right) - H_y^{n+(1/2)}\left(m-\frac{1}{2}\right)\right) \tag{5}$$

$$E_x^{n+1} = \frac{1}{b_0}\left[a_0\left(\frac{D_x^{n+1}}{\varepsilon_0}\right) + a_1\left(\frac{D_x^n}{\varepsilon_0}\right) + a_2\left(\frac{D_x^{n-1}}{\varepsilon_0}\right)\right] - b_1 E_x^n - b_2 E_x^{n-1} \tag{6}$$

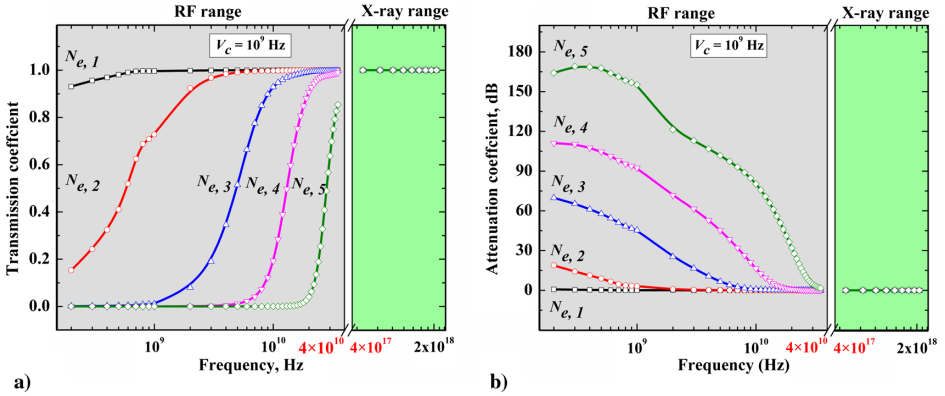

Fig. 2 Representations of a) transmission and b) attenuation coefficients at different carrier frequencies and under various peak electron densities with fixed electron collision frequency.

The constant coefficient in Eq. (6) can be determined by

$$\begin{cases} a_0 = v_c \frac{2}{\Delta t} + \left(\frac{2}{\Delta t}\right)^2 \\ a_1 = 2\left(\frac{2}{\Delta t}\right)^2 \\ a_2 = v_c \frac{2}{\Delta t} + \left(\frac{2}{\Delta t}\right)^2 \end{cases} \tag{7a}$$

$$\begin{cases} b_0 = \omega_p^2 + v_c \frac{2}{\Delta t} + \left(\frac{2}{\Delta t}\right)^2 \\ b_1 = 2\omega_p^2 - 2\left(\frac{2}{\Delta t}\right)^2 \\ b_2 = \omega_p^2 - v_c \frac{2}{\Delta t} + \left(\frac{2}{\Delta t}\right)^2 \end{cases} \tag{7b}$$

On the basis of Eqs. (4–6), E_x could be calculated iteratively. The transmission and attenuation coefficients could be obtained by calculating the E_x value of the EM waves penetrating the plasma sheath. To ensure the validity of the simulation, we guaranteed that spatial step size Δz and temporal step size Δt satisfied the Courant stability condition and numerical dispersion relation [24,25]:

$$c \cdot \Delta t \le \Delta z \tag{8}$$

$$\Delta z \le \lambda/12 \tag{9}$$

In the RF band simulations, Δz and Δt were set to 7.5×10^{-4} m and 2.5×10^{-12} s, respectively. However, if the FDTD method was used for X-ray simulation, then the ultrashort wavelength of the X-ray caused the spatial step to be extremely short to satisfy Eqs. (8) and (9), leading to unacceptably low computational efficiency. Therefore, the theoretical WKB approximation method was used to analyze the interaction between the X-ray and plasma sheath to achieve high computational speed, whereas the FDTD method was used to simulate the RF band to ensure high calculation accuracy.

In the simulation based on the WKB method, we calculated the X-ray propagation in the cold, isotropic, collision, inhomogeneous, and steady-state plasma medium [23]. The frequency range of the incident X-ray was 10^8–10^9 GHz. The electron density satisfied the double exponential distribution, and ε satisfied

Table 1 Peak electron densities of the plasma sheath

Variable	Peak electron density, m^{-3}
$N_{e,1}$	1.99×10^{15}
$N_{e,2}$	6.56×10^{16}
$N_{e,3}$	8.75×10^{17}
$N_{e,4}$	3.50×10^{18}
$N_{e,5}$	1.27×10^{19}

$$\varepsilon = (1 - w_p^2/(w^2 + v_c^2) - (j \cdot v_c/w) \cdot (w_p^2/(w^2 + v_c^2)))\varepsilon_0 \tag{10}$$

Here, k can be given by

$$k = \frac{w}{c}\sqrt{\varepsilon/\varepsilon_0} \tag{11}$$

If the X-ray beam irradiates the plasma slab vertically; then T and Att can be given by

$$T = \exp\left(-2\mathrm{Im}\left(\int_0^{z_1} k\,\mathrm{d}z\right)\right) \tag{12}$$

$$\mathrm{Att} = -10\lg T = 8.686\mathrm{Im}\left(\int_0^{z_1} k\,\mathrm{d}z\right) \tag{13}$$

B. Results and Discussions

The SO-FDTD and WKB methods were used to evaluate the transmission properties of the RF waves and X-ray beams, respectively. With consideration of different peak electron densities and electron collision frequencies, we obtained the transmission and attenuation coefficients of the EM waves, including the RF and X-ray ranges. As shown in Fig. 2, the collision frequency was fixed at 1 GHz, and different peak electron densities were considered. Here, the values of peak electron density are shown in Table 1. In the RF range, the transmission coefficient increased and the attenuation coefficient decreased as the carrier frequency increased. Moreover, a high peak electron density required high carrier frequencies for transmission, thereby indicating that employing high-frequency carriers can mitigate communication blackout. In the X-ray range, the X-rays demonstrated a strong penetrating property and were able to pass through the plasma without attenuation.

Under different electron collision frequencies and fixed peak electron density, the curves of the transmission and attenuation coefficients changed with the carrier frequency (Fig. 3). In the RF range, the electron collision frequency significantly affected the shape of the transmission and attenuation coefficient curves. However, in the X-ray range, the shape of the transmission and attenuation coefficient curves was unaffected by varying electron collision frequency.

III. X-Ray Transmission in the Martian Upper Atmosphere

Communication blackout ordinarily occurs at an altitude of 35–110 km during the Mars atmospheric entry phase [9]. The atmospheric attenuation of X-ray beams depends on the X-ray energy as well as the atmosphere density and composition. The Martian atmosphere is mainly composed of carbon dioxide (CO_2), nitrogen (N_2) and argon (Ar). The density of the Martian atmosphere as a

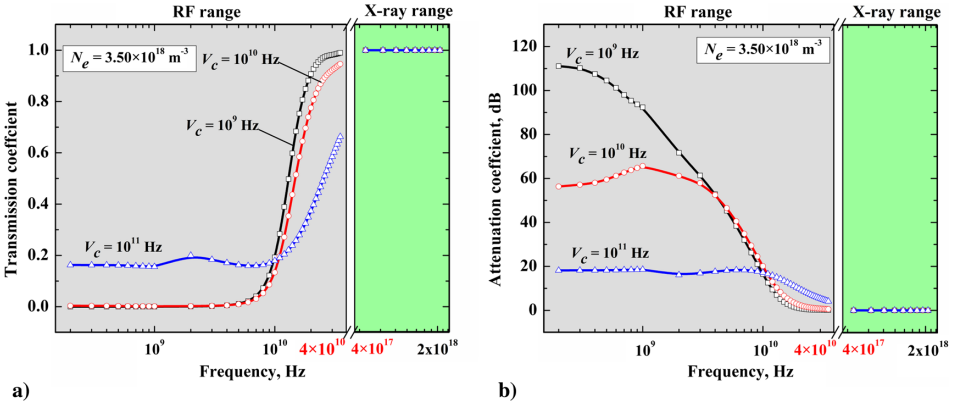

Fig. 3 Representations of a) transmission and b) attenuation coefficients at different carrier frequencies and under various electron collision frequencies with fixed peak electron density.

function of the altitude and the volume percentage of the composition of the Martian atmosphere used in the simulation are shown in Fig. 4 [26].

A. Simulation Method

In this study, the Monte Carlo N-Particle Code Version 5 (MCNP5) was adopted in calculating the X-ray transmission [27]. The propagation process of the X-ray beams with different energies in the Martian atmosphere was simulated with the uplink example. As shown in Fig. 5, the altitude of the orbiter was 225 km [20], and the altitude of the entry vehicle ranged from 35 to 110 km. The Martian atmosphere with altitudes between 35 and 225 km was modeled in the MCNP5 code. As the density of the atmosphere varies with altitude, the atmosphere model was divided into several layers vertically. Moreover, the link angle θ was also considered.

B. Results and Discussions

The transmission coefficients of the X-ray beams with energies ranging from 10 to 90 keV were obtained on the basis of the MCNP5 simulation. The results of the simulations were reported with a relative error of less than 1%. Figure 6 shows the transmission coefficient of the X-ray beams with different energies as a function of the entry vehicle's altitude when the communication blackout occurred and the Mars orbiter was located right above the entry vehicle ($\theta = 0$ deg). The X-ray transmission coefficient gradually decreased as the altitude of the entry vehicle decreased. At the same altitude of the entry vehicle, the X-ray beams with high energy provided a large transmission coefficient, which indicated satisfactory penetration performance. If the entry vehicle was at the bottom of the communication blackout region (height of 35 km), the transmission coefficient could exceed 0.6 when the energy of the X-ray beam was higher than 20 keV. Therefore, in the upper Martian atmosphere, long-range X-ray signal transmission can be achieved with a relatively low X-ray energy (greater than 20 keV). Our calculation results indicate that X-ray beams with energy below 90 keV could provide more than five times the penetration in the Martian upper atmosphere than the Earth's [16].

The transmission profile of the X-ray beams along the uplink path when the link angle was 0 deg and the altitude of the entry vehicle was

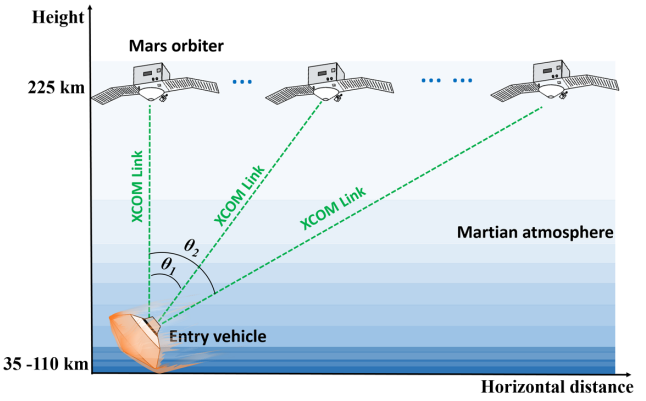

Fig. 5 Schematic of the calculation model for evaluation of the transmission properties of the X-ray beam in the Martian atmosphere.

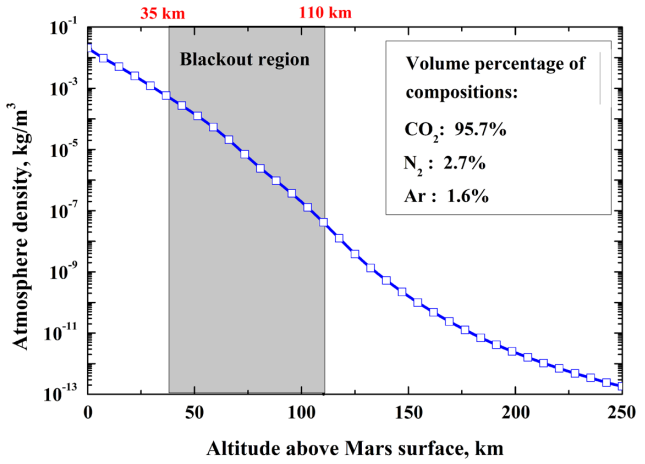

Fig. 4 Density of the Martian atmosphere as a function of altitude and the volume percentage of the composition of the Martian atmosphere.

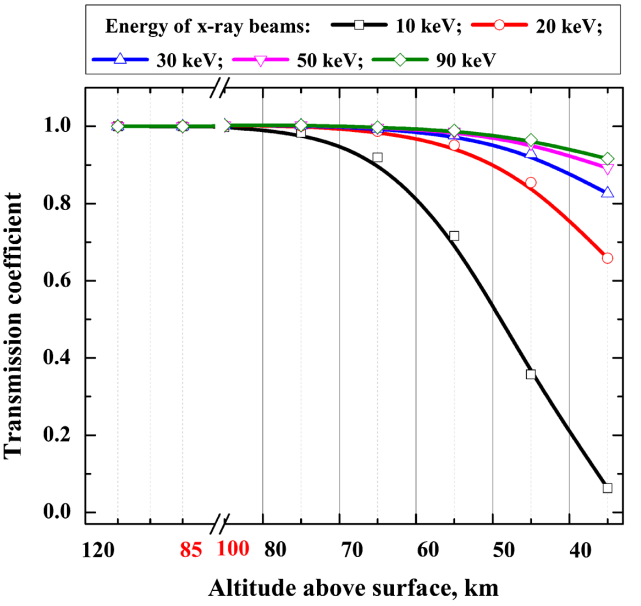

Fig. 6 Transmission coefficients of X-ray beams with different energies under varying entry vehicles' altitudes.

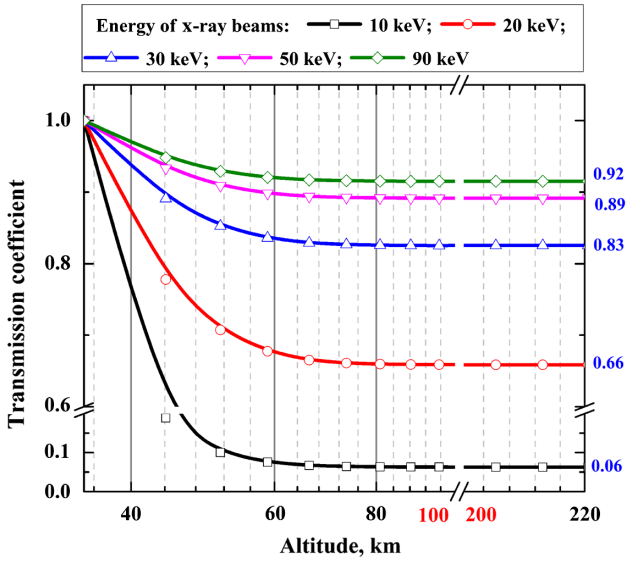

Fig. 7 Transmission coefficients of X-ray beams with different energies along the uplink path under the entry vehicle's altitude of 35 km.

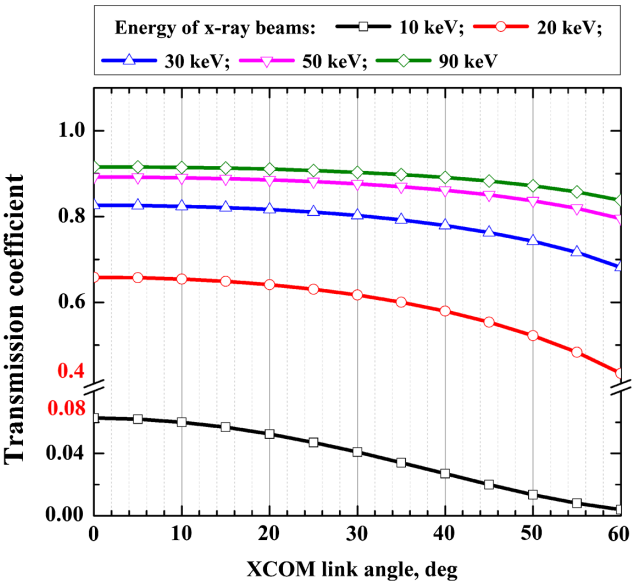

Fig. 8 Transmission coefficients of X-ray beams with different energies under various link angles.

35 km is shown in Fig. 7. With the altitude increasing from 35 to 60 km, the intensity of the X-ray beams gradually declined. However, the atmospheric attenuation can be neglected in the region of 60–220 km. The results indicated that the degree of X-ray attenuation in the Martian atmosphere depends on atmospheric density.

The altitudes of the entry vehicle and obiter were fixed at 35 and 220 km, respectively. The transmission coefficients of the X-ray beams with different energies as a function of the link angle θ are shown in Fig. 8. As a large angle leads to a long propagation path, the transmission coefficients of the X-ray beams gradually decreased as the angle increased. However, for the X-ray beams with energies of up to 30 keV, the link angle did not result in a large decline in the transmission property.

IV. Communication Property Evaluation

A. Simulation Method

The bit error ratio (BER) and signal-to-noise ratio (SNR) are indicators of a communication link. The BER is the number of bit errors divided by the number of transferred bits during a particular time arrival. The SNR is the ratio of the received signal strength over the noise strength in the frequency range of the operation. In this section, the XCOM link from the entry vehicle to the orbiter during the Mars atmospheric entry phase is modeled based on the intensity modulation/direct detection communication system. The atmospheric attenuation, plasma attenuation, and beam divergence of the communication link were considered. The communication performance was then evaluated in the plasma and Martian atmosphere channels by calculating the probability of the BER versus the SNR under wireless channel models.

In this communication link model, the nested X-ray-focusing optics with the efficiency η_c of 70% were used as the transmitting and receiving antenna. The divergence angle θ_d of the X-ray beam output from the transmitting antenna was 3×10^{-3} rad [14], the area of the receiving antenna A_R was 0.25 m^2, and the communication bandwidth B was 10^6 Hz. A silicon drift detector (SDD) with an effective area of 1 cm^2 was employed. Its dark current i_d was 1.5×10^{-10} A [28]. For X-ray photons with energy between 10 and 20 keV, the detection efficiency η was higher than 40%. When the transmitting power is P_T and the communication distance is L, the receiving power P_R can be determined by

$$P_R = A_R P_T C_t \eta_c^2 / \pi \theta_d^2 L^2 \tag{14}$$

where the transmission coefficient C_t represents the absorption of atmosphere and plasma, and its value can be obtained by previous calculation. The SNR value can be determined by [29,30]

$$\mathrm{SNR} = 2(\eta e/h\upsilon)^2 P_R^2 / (3e^2 \eta B(P_R/h\upsilon + F_B) + 2ei_d B) \tag{15}$$

where υ is the X-ray frequency, and F_B is the flux of the background X-ray photon. The value of F_B was set to 50 $m^{-2} \cdot s^{-1}$ in this calculation [31]. According to the SNR value, the BER of the XCOM system with on–off keying (OOK) and the pulse position modulation (PPM) method can then be obtained by Eqs. (16) and (17), respectively [32]:

$$\mathrm{BER}_{\mathrm{OOK}} = \frac{1}{2}\mathrm{erfc}\left(\frac{1}{2\sqrt{2}}\sqrt{\mathrm{SNR}}\right) \tag{16}$$

$$\mathrm{BER}_{\mathrm{PPM}} = \frac{1}{2}\mathrm{erfc}\left(\frac{1}{2\sqrt{2}}\sqrt{\mathrm{SNR}\frac{M}{2}\log_2 M}\right) \tag{17}$$

where M is the modulation level of the PPM method, and the 4-level-PPM method was adopted in this calculation.

B. Results and Discussions

We evaluated the communication performance of the links between the entry vehicle and the Mars obiter when the flight altitude of the entry vehicle was from 120 to 35 km and θ was 0 deg. The SNR curves of XCOM links as a function of the entry vehicle's altitude are shown in Fig. 9. Figure 9a shows the SNR result of different energy links with a fixed transmitting power of 10 W. The beam attenuation caused by atmospheric absorption and geometric spread increases rapidly as the altitude of the entry vehicle decreases, which leads to the rapid decrease in the SNR value. XCOM links with X-ray energy of 10 and 20 keV provide better SNR performance than the links with higher energies, although higher-energy links have lower atmospheric attenuation. This is because the detector we employed in this evaluation has an X-ray detection efficiency peak of about 10 keV. The XCOM link with an X-ray energy of 10 keV has a good SNR performance when entry vehicle's altitude is above 40 km. However, at altitudes below 40 km, the link with an X-ray energy of 20 keV is needed to make it easier to penetrate the Martian atmosphere. The SNR results of different transmitting power links with a fixed X-ray energy of 20 keV are shown in Fig. 9b. For a certain altitude, higher transmitting power can provide a higher SNR value, which means better communication performance.

On the basis of the SNR results, the BER performance of the OOK- and PPM-modulated links during the Mars entry phase was analyzed. The BER curves of the link based on OOK and PPM modulation

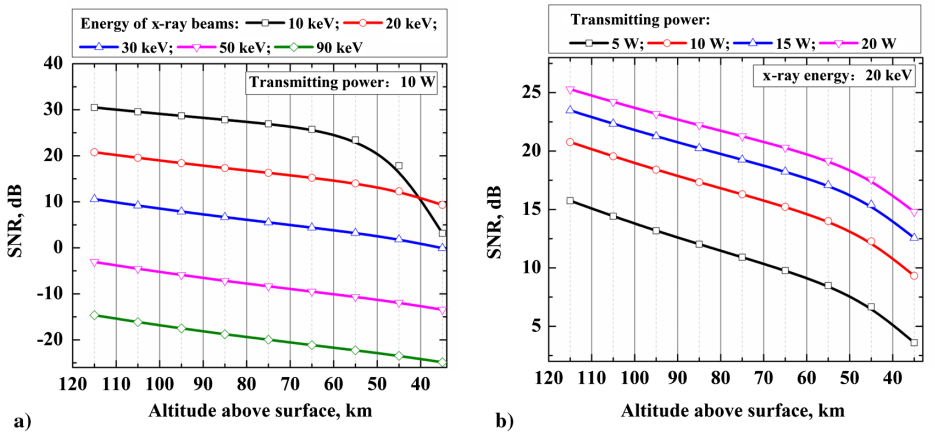

Fig. 9 SNR of the XCOM links with a) different X-ray energies and b) different transmitting powers under varying entry vehicle's altitude.

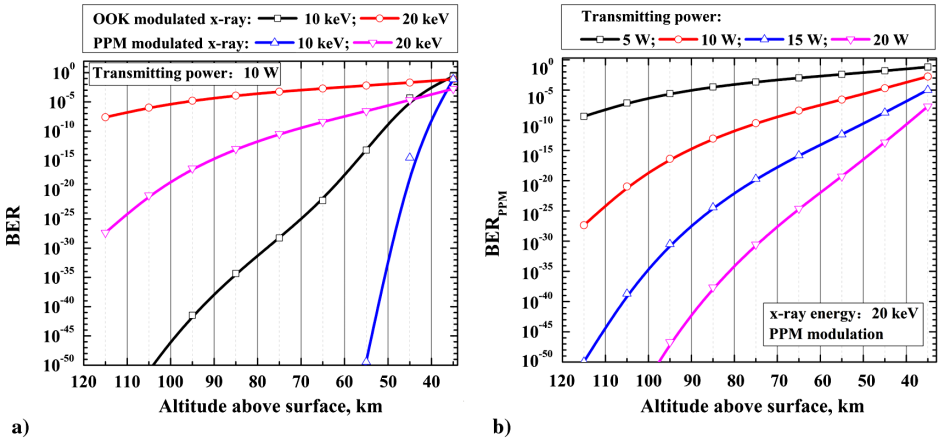

Fig. 10 BER of XCOM links with a) different X-ray energies and b) different transmitting powers under varying entry vehicle's altitude.

methods are shown in Fig. 10a. For the same SNR conditions, PPM-modulated X-ray beams can provide lower BER than OOK-modulated beams. BER curves of 20-keV X-ray links based on the 4-PPM modulation method with different transmitting powers are shown in Fig. 10b. The BER value increases significantly with the decrease of the entry vehicle's altitude. Obviously, improving transmitting power can reduce the BER value of the XCOM link. Moreover, in the Mars entry scenarios, the 20-keV X-ray link with a transmitting power of 15 W can ensure that the BER is less than 10^{-5}.

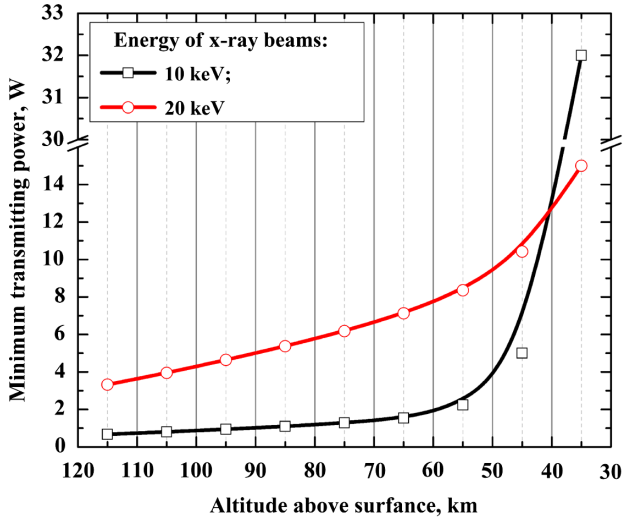

Fig. 11 Minimum transmitting power required for low BER XCOM under varying entry vehicle's altitude.

The minimum transmitting power required to achieve the BER of less than 10^{-5} as a function of the entry vehicle's altitude was calculated, and the results of the links with the X-ray energies of 10 and 20 keV are shown in Fig. 11. The minimum transmitting power requirement increases as the entry vehicle's altitude decreases. To achieve low BER XCOM during Mars entry, the 10- and 20-keV X-ray links require the transmitting power of 32 and 15 W, respectively. Moreover, 10- and 20-keV X-ray links are suitable before and after the entry vehicle drops to an altitude of 40 km.

V. Conclusions

This study provides a demonstration of the potential application of X-ray communication for communication blackout during the Mars atmospheric entry phase. On the basis of the finite difference time domain and Wentzel–Kramer–Brillouin methods, the X-ray transmission properties in the plasma sheath were evaluated and compared with the transmission properties of RF bands. The X-ray beams exhibited significantly stronger penetration performance than the RF bands and penetrated the plasma sheath without attenuation. Moreover, the transmission properties of X-ray beams in the Martian atmosphere were evaluated based on the Monte Carlo Particle Transport Program Version 5 code. When X-ray energy was higher than 20 keV, a transmission coefficient of more than 0.6 could be achieved. This result indicates that X-ray communication links could be established between the entry vehicle and the orbiter in the blackout region without significant signal attenuation. In addition, the X-ray communication performance in the Mars blackout region was evaluated. The results indicate that the X-ray link with the energy of 20 keV and the transmitting power of 15 W could achieve the bit error rate of less than 10^{-5}.

Acknowledgments

This work was supported by the China Postdoctoral Science Foundation (no. 2016M601807), the Fundamental Research Funds for the Central Universities (nos. NP2018408 and NT2018017), the Postgraduate Research and Practice Innovation Program of Jiangsu Province (no. KYCX18_0271), the General Technology and Field Fund for Equipment Pre-Research (no. JZX7Y20190258057701), the State Key Laboratory of Simulation and Effects of Intense Pulse Radiation Environment (no. SKLIPR1813), the Special Foundation of China Postdoctoral Science Foundation (no. 2018T110500), and the Nanjing University of Aeronautics and Astronautics Ph.D. Short-Term Visiting Scholar Project (no. 190406DF06).

References

[1] Edquist, K. T., Desai, P. N., and Schoenenberger, M., "Aerodynamics for Mars Phoenix Entry Capsule," *Journal of Spacecraft and Rockets*, Vol. 48, No. 5, 2011, pp. 713–726. doi:10.2514/1.46219

[2] Tauber, M. E., Bowles, J. V., and Yang, L., "Use of Atmospheric Braking During Mars Missions," *Journal of Spacecraft and Rockets*, Vol. 27, No. 5, 1990, pp. 514–521. doi:10.2514/3.26174

[3] Lightsey, E. G., Mogensen, A. E., Burkhart, P. D., Ely, T. A., and Duncan, C., "Real-Time Navigation for Mars Missions Using the Mars Network," *Journal of Spacecraft and Rockets*, Vol. 45, No. 3, 2008, pp. 519–533. doi:10.2514/1.30974

[4] Kim, M., and Boyd, I. D., "Effectiveness of a Magnetohydrodynamics System for Mars Entry," *Journal of Spacecraft and Rockets*, Vol. 49, No. 6, 2012, pp. 1141–1149. doi:10.2514/1.A32256

[5] Morabito, D., Schratz, B., Bruvold, K., IIott, P., Edquist, K., and Cianciolo, A. D., "The Mars Science Laboratory EDL Communications Brownout and Blackout at UHF," Interplanetary Network Progress Rept. 42–197, Jet Propulsion Lab., California Inst. of Technology, Pasadena, CA, 2014.

[6] Nordgard, J. D., "A Martian Entry Propagation Study," *Radio Science*, Vol. 11, No. 11, 1976, pp. 947–957. doi:10.1029/RS011i011p00947

[7] Kim, M., Boyd, I. D., and Keidar, M., "Modeling of Electromagnetic Manipulation of Plasmas for Communication During Reentry Flight," *Journal of Spacecraft and Rockets*, Vol. 47, No. 1, 2010, pp. 29–35. doi:10.2514/1.45525

[8] Kim, M., Keidar, M., and Boyd, I. D., "Analysis of an Electromagnetic Mitigation Scheme for Reentry Telemetry Through Plasma," *Journal of Spacecraft and Rockets*, Vol. 45, No. 6, 2008, pp. 1223–1229. doi:10.2514/1.37395

[9] Morabito, D., "The Spacecraft Communications Blackout Problem Encountered During Passage or Entry of Planetary Atmospheres," Interplanetary Network Progress Rept. 42-150, Jet Propulsion Lab., California Inst. of Technology, Pasadena, CA, 2002.

[10] Hang, S., Liu, Y. P., Li, H., Tang, X. B., and Chen, D., "Temporal Characteristic Analysis of Laser-Modulated Pulsed X-Ray Source for Space X-Ray Communication," *Nuclear Instruments and Methods in Physics Research Section A: Accelerators, Spectrometers, Detectors and Associated Equipment*, Vol. 887, April 2018, pp. 18–26. doi:10.1016/j.nima.2018.01.031

[11] Lévesque, J. F., and Lafontaine, J. D., "Innovative Navigation Schemes for State and Parameter Estimation During Mars Entry," *Journal of Guidance, Control, and Dynamics*, Vol. 30, No.1, 2007, pp. 169–184. doi:10.2514/1.25107

[12] Burkhart, P., Ely, T., Duncan, C., Lightsey, E., Campbell, T., and Mogensen, A., "Expected EDL Navigation Performance with Spacecraft to Spacecraft Radiometric Data," *AIAA Guidance, Navigation, and Control Conference and Exhibit*, AIAA Paper 2005-5949, 2005. doi:10.2514/6.2005-5949

[13] Hastrup, R. C., Bell, D. J., Cesarone, R. J., Edwards, C. D., Ely, T. A., Guinn, J. R., Rosell, S. N., Srinivasan, J. M., and Townes, S. A., "Mars Network for Enabling Low-Cost Missions," *Acta Astronaut*, Vol. 52, Nos. 2–6, 2003, pp. 227–235. doi:10.1016/S0094-5765(02)00161-3

[14] Liu, D., Qiang, P. F., Li, L. S., Su, T., Sheng, L. Z., Liu, Y. A., and Zhao, B. S., "X-Ray Focusing Optics and Its Application in X-Ray Communication System," *Acta Physica Sinica*, Vol. 65, No. 1, 2016, Paper 010703. doi:10.7498/aps.65.010703

[15] Liu, Y. P., Li, H., Li, Y. L., Hang, S., and Tang, X. B., "Transmission Properties and Physical Mechanisms of X-Ray Communication for Blackout Mitigation During Spacecraft Reentry," *Physics of Plasmas*, Vol. 24, No. 11, 2017, Paper 113507. doi:10.1063/1.4998786

[16] Li, H., Tang, X. B., Hang, S., Liu, Y. P., and Chen, D., "Potential Application of X-Ray Communication Through a Plasma Sheath Encountered During Spacecraft Reentry into Earth's Atmosphere," *Journal of Applied Physics*, Vol. 121, No. 12, 2017, Paper 123101. doi:10.1063/1.4978758

[17] Dunn, M. G., and Kang, S., "Theoretical and Experimental Studies of Reentry Plasmas," NASA CR-2232, 1973.

[18] Bai, B. W., Li, X. P., Liu, Y. M., and Xu, J., "Effects of Reentry Plasma Sheath on Mutual-Coupling Property of Array Antenna," *International Journal of Antennas and Propagation*, Vol. 2015, 2015. Paper 542392. doi:10.1155/2015/542392

[19] Gillman, E., Foster, J., and Blankson, I., "Review of Leading Approaches for Mitigating Hypersonic Vehicle Communications Blackout and a Method of Ceramic Particulate Injection via Cathode Spot Arcs for Blackout Mitigation," NASA TM-2010-216220, 2010.

[20] Morabito, D., and Edquist, K. T., "Communications Blackout Predictions for Atmospheric Entry of Mars Science Laboratory," *2005 IEEE Aerospace Conference Proceedings*, IEEE Publ., Piscataway, NJ, 2005, pp. 489–500. doi:10.1109/AERO.2005.1559339

[21] Yang, H. W., and Chen, R. S., "FDTD Analysis on the Effect of Plasma Parameters on the Reflection Coefficient of the Electromagnetic Wave," *Optical and Quantum Electronics*, Vol. 39, No. 15, 2007, pp. 1245–1252. doi:10.1007/s11082-008-9195-8

[22] Takahashi, Y., Yamada, K., and Abe, T., "Examination of Radio Frequency Blackout for an Inflatable Vehicle During Atmospheric Reentry," *Journal of Spacecraft and Rockets*, Vol. 51, No. 2, 2014, pp. 430–441. doi:10.2514/1.A32539

[23] Ratowsky, R. P., and London, R. A., "Propagation of Mutual Coherence in Refractive X-Ray Lasers Using a WKB Method," *Physical Review A:* General Physics, Vol. 51, No. 3, 1995, pp. 2361–2370. doi:10.1103/PhysRevA.51.2361

[24] Martin, T., and Pettersson, L., "Dispersion Compensation for Huygens' Sources and Far-Zone Transformation in FDTD," *IEEE Transactions on Antennas and Propagation*, Vol. 48, No. 4, 2000, pp. 494–501. doi:494-501.10.1109/8.843662

[25] Schneider, J. B., and Kruhlak, R. J., "Dispersion of Homogeneous and Inhomogeneous Waves in the Yee Finite-Difference Time-Domain Grid," *IEEE Transactions on Microwave Theory and Techniques*, Vol. 49, No. 2, 2001, pp. 280–287. doi:10.1109/22.903087

[26] MCD, Mars Climate Database [online database], Ver. 5.3, European Space Agency, Paris, France, 2018, http://www-mars.lmd.jussieu.fr/mars/access.html [retrieved 25 Oct. 2018].

[27] Kiedrowski, B., Booth, T., Brown, F., Bull, J., Favorite, J., Forster, R., and Martz, R., "MCNP5-1.6, Feature Enhancements and Manual Clarifications," Los Alamos National Lab. LA-UR-l0-06217, Los Alamo, NM, 2010.

[28] Hansen, K., and Christian, R., "Noise Analysis of an Si-Drift Detector System with Time-Variant Shaping," *IEEE Transactions on Nuclear Science*, Vol. 51, No. 6, 2004, pp. 3845–3852. doi:10.1109/TNS.2004.839369

[29] Ghassemlooy, Z., Popoola, W., and Rajbhandari, S., *Optical Wireless Communications: System and Channel Modelling with Matlab*, CRC Press, Boca Raton, FL, 2012, pp. 347–394.

[30] Zhang, W. D., Li, H. Z., Wang, Z. J., Tang, Y. F., and Liu, R. C., "Link Identity Analysis and Power Budget for Deep Space Optical Communications," *Journal of Air Force Engineering University*, Vol. 12, No. 6, 2011, pp. 55–60. doi:10.1097/IGC.0b013e31820fa168

[31] Wei, E., Jin, S., Zhang, Q., Liu, J., Li, X., and Yan, W., "Autonomous Navigation of Mars Probe Using X-Ray Pulsars: Modeling and Results," *Advances in Space Research*, Vol. 51, No. 5, 2013, pp. 849–857. doi:10.1016/j.asr.2012.10.009

[32] Elganimi, T. Y., "Studying the BER Performance, Power- and Bandwidth-Efficiency for FSO Communication Systems Under Various Modulation Schemes," *2013 IEEE Jordan Conference on Applied Electrical Engineering and Computing Technologies*, IEEE Publ., Piscataway, NJ, 2013, pp. 1–6. doi:10.1109/AEECT.2013.6716426

K. T. Edquist
Associate Editor